Molecular Rayleigh scattering diagnostic for measurement of high frequency temperature fluctuations

Amy F. Mielke[a], Kristie A. Elam[b]

[a]NASA Glenn Research Center, 21000 Brookpark Road, Cleveland, OH, USA 44135;
[b]Jacobs Sverdrup, 21000 Brookpark Road, Cleveland, OH, USA 44135

ABSTRACT

A novel technique for measurement of high frequency temperature fluctuations in unseeded gas flows using molecular Rayleigh scattering is investigated. The spectrum of laser light scattered from molecules in a gas flow is resolved using a Fabry-Perot interferometer. The width of the spectral peak is broadened by thermal motion of the molecules and hence is related to gas temperature. The interference fringe pattern containing spectral information is divided into four concentric regions using a series of mirrors angled with respect to one another. Light from each of these regions is directed towards photomultiplier tubes and sampled at 10 kHz using photon counting electronics. Monitoring the relative change in intensity within each region allows measurement of gas temperature. Independently monitoring the total scattered intensity provides a measure of gas density. This technique also has the potential to simultaneously measure a single component of flow velocity by monitoring the spectral peak location. Measurements of gas temperature and density are demonstrated using a low speed heated air jet surrounded by an unheated air co-flow. Mean values of temperature and density are shown for radial scans across the jet flow at a fixed axial distance from the jet exit plane. Power spectra of temperature and density fluctuations at several locations in the jet are also shown. The instantaneous measurements have fairly high uncertainty; however, long data records provide highly accurate statistically quantities, which include power spectra. Mean temperatures are compared with thermocouple measurements as well as the temperatures derived from independent density measurements. The accuracy for mean temperature measurements was +/- 7 K.

Keywords: Rayleigh scattering, temperature fluctuation measurement, Fabry-Perot interferometer

1. INTRODUCTION

A molecular Rayleigh scattering technique is developed to measure dynamic gas temperature and density in unseeded turbulent flows at high sampling rates (10 kHz). A high power CW laser beam is focused at a point in a heated jet plume and Rayleigh scattered light is collected and spectrally resolved. The spectrum of the light contains information about the temperature, velocity, and density of the flow. A planar mirror Fabry-Perot interferometer (FPI) is used to analyze the spectrum of the scattered light, and photomultiplier tubes (PMTs) record the spectra at high sampling rates and allow dynamic measurement of the gas flow properties. Mean values of temperature and density, as well as power spectra of the flow property fluctuations are presented for measurements in a low speed heated air jet.

There is currently no high frequency response, non-intrusive temperature measurement technique for use in turbulent flow studies. There are also no techniques that can provide non-intrusive dynamic measurement of gas temperature, velocity, and density simultaneously. Conventional intrusive measurement devices such as hot wires, pressure probes, and thermocouples are usually limited in spatial and temporal response, disturb the flow under study, and can be damaged by high pressure or temperature. The non-intrusive technique presented here can provide data particularly useful to aeroacoustics researchers who are interested in correlating flow property fluctuations with far field acoustic fluctuations. Knowledge of velocity-temperature fluctuation correlations is also needed to improve computational fluid dynamic (CFD) models of compressible turbulent flows.

Various optical techniques are available for temperature and species concentration measurements. Eckbreth[1] provides the details of several of these techniques, such as Coherent Anti-Stokes Raman Spectroscopy (CARS), Spontaneous Raman and Rayleigh scattering, and Laser-Induced Fluorescence (LIF), along with the advantages and disadvantages of each.

CARS and LIF require complex setups, involving multiple lasers. Raman scattering requires only a single laser wavelength, however the method suffers from weak signal strength. Another technique called Laser-Induced Thermal Acoustics (LITA)[2,3], also known as Transient Grating Spectroscopy (TGS)[4], is a point-wise technique that measures instantaneous temperature, velocity, and species concentrations. This technique requires the use of two high-energy pulsed laser beams to generate a dynamic refraction index grating in the medium, as well as a low-power probe laser beam. The temporal response of these techniques is typically limited by the repetition rate of pulsed lasers, usually on the order of 10 Hz, or the signal strength of the scattering process.

Rayleigh scattering has several advantages over other light scattering techniques. The Rayleigh scattering cross-section is 3 orders of magnitude greater than the Raman scattering cross-section. Also, Rayleigh techniques are generally much simpler to implement than techniques that require multiple lasers and other complicating factors. Previous works using molecular Rayleigh scattering to make temperature, velocity, and number density measurements in harsh environments have been reported[5-8]. The current work is an extension of a previously developed technique using Rayleigh scattering to obtain dynamic density and velocity measurements in supersonic free jets[9,10].

2. THEORY

2.1. Rayleigh scattering and spectral analysis

Molecular Rayleigh scattering is the result of elastic light scattering from gas molecules. When light from a single frequency laser beam passes through a gas, the scattered light is shifted in frequency by the Doppler effect due to the thermal as well as the bulk motion of the molecules. The frequency spectrum of the scattered light contains information about the gas density, bulk velocity, and temperature. Figure 1 shows a Rayleigh scattering spectrum containing the narrow laser line and the Rayleigh spectral peak for 90° scattering and air flowing at 300 m/s with temperature 250 K and pressure 1.8 atm. If the gas composition is fixed, the total intensity of the Rayleigh scattered light is directly proportional to the gas density. The frequency shift between the laser peak and the Rayleigh peak is proportional to the bulk flow velocity. The width of the spectrum is related to the gas temperature.

The shape of the spectrum is dependent on gas pressure, temperature and the scattering angle[11]. A non-dimensional parameter y, which represents the ratio of the wavelength of molecular fluctuations to the mean free path between molecular collisions, is used to establish spectral shape regimes:

$$y = \frac{p}{\eta K a} \tag{1}$$

where p is the gas pressure, η is the gas viscosity, K is the magnitude of the interaction wave vector $\mathbf{K}$ that defines the direction of the velocity component, u_k, being measured, and a is the most probable molecular speed defined as

$$a = \sqrt{\frac{2\kappa T}{m}} \tag{2}$$

where κ is the Boltzmann constant, T is the fluid temperature, and m is the molecular mass. The interaction wave vector is the bisector of the incident and scattered light wave vectors (figure 2). The interaction wave vector and its magnitude are given by:

$$\mathbf{K} = \mathbf{k_s} - \mathbf{k_0} \tag{3}$$

$$K = |\mathbf{K}| = \frac{4\pi}{\lambda}\left[\sin\frac{\chi_s}{2}\right] \tag{4}$$

where λ is the wavelength of the incident light and χ_s is the scattering angle between the incident ($\mathbf{k_0}$) and scattered ($\mathbf{k_s}$) light wave vectors. The geometry of the optical arrangement in an experiment can be designed such that the desired component of the velocity is measured:

$$u_k = \frac{\mathbf{K} \cdot \mathbf{u}}{K} \tag{5}$$

Three spectral shape regimes are defined for typical 90° scattering[11-13]. For low density gases where $y \ll 1$, the Rayleigh spectrum is accurately modeled by a Gaussian function and the gas is said to be in the Knudsen or collisionless regime. For higher density gases where $y \gg 1$, the Rayleigh spectrum broadens and eventually develops side-lobes known as

Brillouin peaks. This is known as the hydrodynamic or continuum regime where molecular collisions are the dominant process. Finally, for $0.2 \leq y \leq 2$, as is the case in the present experiments, the gas is in a transition region between the collisionless and hydrodynamic regimes, and a kinetic theory model is required. The shape regimes are illustrated in figure 3. A model developed by G. Tenti[11,14] provides a kinetic model of Rayleigh-Brillouin scattering from molecular gases in all density regimes. The TENTI S6 spectrum model was used to generate the information displayed in figures 1 and 3, and also in the uncertainty analysis discussed in Sec. 2.2.
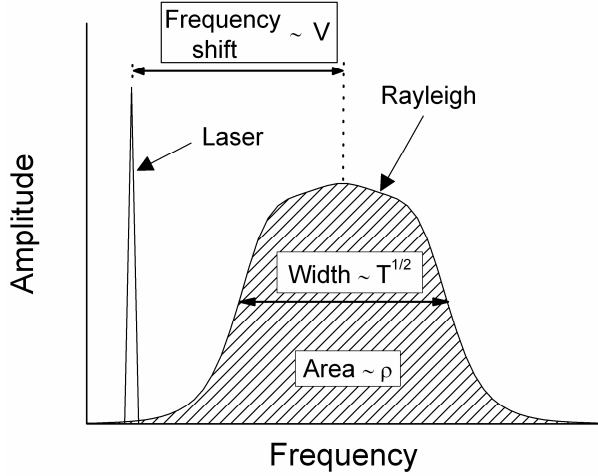

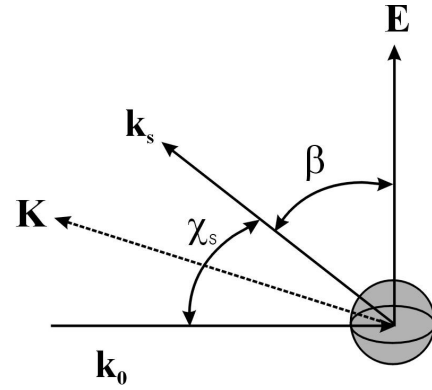Figure 1. Rayleigh scattering spectrum

Figure 2. Light scattering from a moving particle.

The spectrum of the Rayleigh scattered light is analyzed using a planar mirror Fabry-Perot interferometer (figure 4) operated in the static imaging mode[15]. The fringes at the FPI output are focused by a lens. The fringe intensity pattern is a function of the Rayleigh spectrum, S_R, and the Fabry-Perot instrument function, I_{FP}. The image of the fringe pattern is separated into concentric circular and annular areas, which are then sampled using photon counting detection equipment. The Fabry-Perot instrument function is:

$$I_{FP}(x_f, r) = \frac{1}{1 + F \sin^2 \frac{\psi(x_f, r)}{2}} \tag{6}$$

where $F = \dfrac{1}{\sin^2\left(\dfrac{\pi}{2N_e}\right)}$, $\tag{7}$

ψ is the phase change of the light between successive reflections given by:

$$\psi = \frac{4\pi \mu d}{\lambda} \left[\frac{\theta_R^2 - \theta^2}{2} + \frac{\lambda a}{c\Lambda} x_f \right], \tag{8}$$

N_e is the effective finesse, μ is the refractive index of the medium in the Fabry-Perot cavity, d is the Fabry-Perot mirror spacing, $\Lambda = 2\pi/K$, θ is the angle between a light ray incident on the image plane and the optical axis ($\theta = r/f_L$), r is the radial position in the image plane, f_L is the fringe forming lens focal length, θ_R is the angle associated with the fringe radius of the reference laser light r_R, and x_f is the dimensionless frequency defined as

$$x_f = \frac{2\pi(f - f_0)}{Ka}, \tag{9}$$

where $f - f_0$ is the frequency shift between the reference laser light and the Rayleigh scattered light.
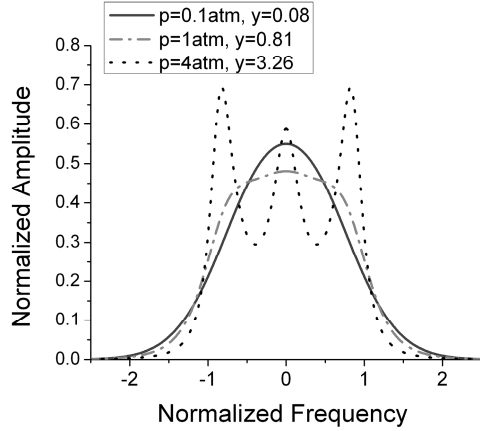
Figure 3. Rayleigh spectrum as a function
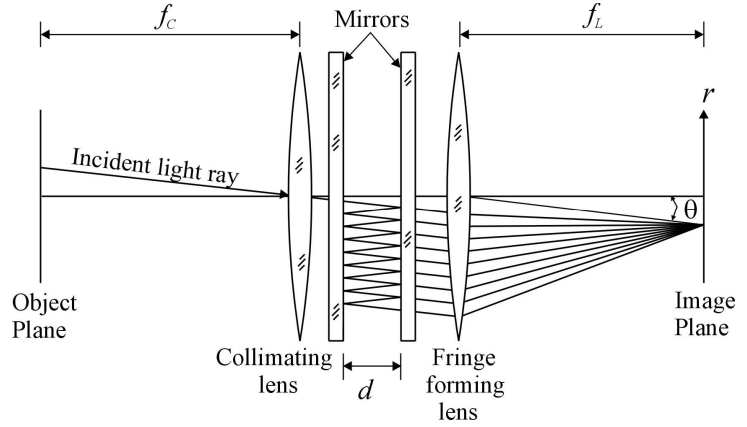of frequency for various y-parameter values.

Figure 4. Fabry-Perot interferometer.

In our experiment, Rayleigh scattered light from a defined probe volume is collected into a multimode optical fiber. The fiber directs the light to the FPI and a lens at the interferometer output focuses the interference fringe pattern at the image plane. The total expected number of Rayleigh photoelectron counts *without* the FPI in the optical path can be expressed as:

$$\langle N_R \rangle = \frac{\varepsilon\, P_0\, n\, L_x\, \lambda\, \Omega\, \Delta t}{h\,c} \left(\frac{d\sigma}{d\Omega} \right) \sin^2 \beta \tag{10}$$

where ε is the overall system efficiency including detector quantum efficiency and other losses, P_0 is the power of the incident laser beam, n is the molecular number density, L_x is the probe volume length, Ω is the light collection solid

angle, Δt is the data acquisition time, $\left(\dfrac{d\sigma}{d\Omega} \right)$ is the differential scattering cross-section of the gas molecules, β is the

angle between the incident electric field vector $\mathbf{E}$ and the scattered light wave vector $\mathbf{k_s}$ (figure 2), h is Planck's constant, and c is the speed of light. When the interferometer is placed in the light path, assuming uniform illumination over the fiber face, the model function for the amount of energy collected on the qth annular region of the detector (containing the interference pattern), in terms of photon counts, can be expressed as follows:

$$\langle N_q \rangle = \frac{\langle N_R \rangle}{\pi\, r_{max}^2} \int\limits_{r_q}^{r_q + \Delta r} \int\limits_{-\infty}^{\infty} S_R(x_f)\, I_{FP}(x_f, r)\, dx_f\, dr \tag{11}$$

where Δr is the width of the annular region, r_{max} is the radius of the image of the fiber face, S_R is the Rayleigh spectrum evaluated using the TENTI S6 model, r_q is the inner radius of the qth annular region. In this work, the fringe pattern is dissected into one circular and three annular regions, and the light in each region is detected using PMTs.

2.2. Lower bound for measurement uncertainty

The lower bound on the uncertainty in velocity, density, and temperature measurements using Rayleigh scattering is set by the photon statistical (shot) noise. Estimates of the measurement uncertainty in the unknown parameters for this technique were obtained by Cramer-Rao lower bound analysis[16]. For a measurement that is a function of a set of unknown parameters, $\hat{\alpha}_i$, the variance of the estimates of the parameters is:

$$V(\hat{\alpha}_i) = \left[\Gamma^{-1} \right]_{ii} \tag{12}$$

where Γ is the Fisher information matrix, which for Poisson statistics is given by:

$$\Gamma_{i,j} = \sum_q \frac{1}{\langle N_q \rangle} \frac{\partial \langle N_q \rangle}{\partial \alpha_i} \frac{\partial \langle N_q \rangle}{\partial \alpha_j} \tag{13}$$

Using the model function developed for $\langle N_q \rangle$, the uncertainty or standard deviation $\sigma(\hat{\alpha}_i)$ in each unknown parameter may be determined by calculation and inversion of the Fisher information matrix.

If a Gaussian spectrum is assumed, the lower bounds for uncertainties in density ρ, temperature T, and velocity u_k for an ideal instrument are:

$$\frac{\sigma(\rho)}{\rho} = \left(\frac{1}{\langle N_R \rangle} \right)^{1/2}$$

$$\frac{\sigma(T)}{T} = \left(\frac{2}{\langle N_R \rangle} \right)^{1/2} \tag{14}$$

$$\sigma(u_k) = \frac{a}{\left(2\langle N_R \rangle \right)^{1/2}}$$

For air flow at zero velocity and temperature 425 K, the lower bound uncertainty estimates for density, temperature, and velocity sampled at 10 kHz, assuming an ideal instrument, are:

$$\frac{\sigma(\rho)}{\rho} = 1.5\%$$

$$\frac{\sigma(T)}{T} = 2.1\%$$

$$\sigma(u_k) = 5.1\,\text{m/s}$$

For any real instrument, these measurement uncertainties will be higher. The Cramer-Rao lower bound measurement uncertainties for the Fabry-Perot interferometer and PMTs in the current system, including overall efficiency of the system, are shown in figure 5. The uncertainty in temperature and density are calculated assuming a known velocity of 0 m/s and sampling rate of 10 kHz. The measurement uncertainty in both temperature and density increases as temperature increases. This is attributable to a lower gas density at higher temperatures, resulting in less scattering molecules, and hence fewer scattered photons. Although the uncertainty in temperature is rather high for instantaneous measurements, long data records can provide highly accurate statistical quantities such as the power spectra of fluctuations. As sampling rates decrease, so will uncertainties, since the uncertainty is inversely related to the total number of photon counts, as shown in Equations 14.
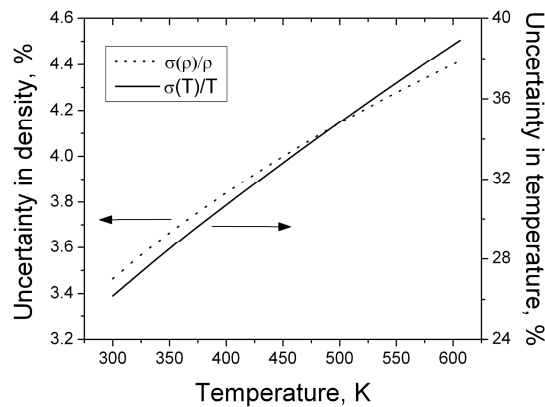

Figure 5. Uncertainty in density and temperature measurements as a function of temperature.

3. EXPERIMENT

Flow measurements were performed downstream of a heated air jet with an 8 mm exit diameter surrounded by a 50 mm diameter 1 m/s room temperature co-flow at the NASA Glenn Research Center using the described Rayleigh scattering measurement technique. The heated air jet is operated over a static temperature range of 298 to 550 K with a mean centerline velocity of 4.8 m/s ± 0.5 m/s measured at an axial distance of 15 mm from the jet exit. Since the measurement technique relies on having particulate free gas flows, a series of filters are placed in line with the air plumbing to remove dust, oil and water from both air supplies. Figure 6a shows the layout of the optics around the jet, which are used to collect Rayleigh scattered light resulting from incident laser light interacting with gas molecules in the jet flow. A 5W, 532 nm, single-frequency, Nd:Vanadate CW laser provides incident light for the system. The laser beam is focused with a 200 mm focal length lens (L1) to a 60 μm $1/e^2$ diameter at the probe volume positioned 15 mm downstream of the jet exit. The beam is oriented in the horizontal direction, perpendicular to the flow direction. The collection optics are arranged such that light is collected at a 90° scattering angle, and focused by a pair of f/3.33, 160 mm focal length lenses (L2, L3) onto a 0.55 mm diameter multimode optical fiber. Since the pair of equal focal length lenses provides 1:1 imaging, the length of the probe volume is 0.55 mm. The incident and scattering wave vectors are arranged such that the radial component of the jet velocity is measured.

The fiber is routed to a separate optical table where spectral analysis and detection takes place, shown in figure 6b. The light exiting the fiber is collimated by an 80 mm focal length lens (L4) and is directed through the planar mirror FPI. The interferometer has 70 mm diameter mirrors with 80% reflectivity, 8.7 GHz free spectral range (FSR), and reflective finesse ≈ 14. The FPI consists of an etalon, or two perfectly parallel mirrors, whose spacing determines the free spectral range. The Fabry-Perot is an extremely sensitive instrument; even the smallest vibrations or temperature changes can cause the mirrors to drift out of parallel alignment. If this happens, the spectral measurements will have increased uncertainty. Therefore, a stabilization routine is utilized to maintain parallelism of the mirrors during testing. Between Rayleigh scattering measurements, a mirror and diffuser (figure 6a) are placed in the beam path by linear actuators to direct some of the incident laser beam into the optical fiber and through the FPI. A set of reflecting prisms mounted on a linear actuator at the output of the interferometer (figure 6b) is positioned in the optical path to direct the light output from three regions of the interferometer mirrors into a video camera. The live video of the three fringe images is used in a feedback control loop to adjust the mirror positions using piezoelectric transducers until the three fringes are equal in diameter. This system is also used to set the fringe diameter of the incident reference light. Further details regarding the mirror stabilization system for the FPI can be found in Reference 10.

When collecting flow measurement data the prisms, mirror, and diffuser are removed from the optical path and the light exiting the FPI is focused by a fringe forming lens (L5) having an effective focal length of 5236 mm, which provided an 18 mm diameter image of the fiber face. The light is sampled via a system of concentric mirrors, referred to as image dissectors. Each image dissector consists of two concentric mirrors, one 25 mm diameter and the other 10 mm diameter, angled with respect to each other such that the incident light containing the intensity pattern is divided into a circular and an annular section and sent in different directions. The combination of three image dissectors and the lenses that focus the light at each dissector (L5-L11) divides the fringe into one circular plus three annular regions. The light from each region is focused onto PMTs, labeled 1-4 in figure 6b. Figure 7 illustrates the individual areas of the fringe image which are directed towards each PMT after the light has passed through the three image dissectors. The angle between the incoming light path and the two outgoing light paths for each image dissector ranged between 18° to 37°. Some light is lost in the process of dissecting the fringe due to shadows created by the small mirror positioned in front of the large mirror. Figure 8 shows a radial slice of a fringe pattern. The areas detected by each PMT are indicated, with the spaces between areas representing the lost light associated with the thickness and angle of the small mirror. The PMTs are operated in the photon counting mode to acquire fringe intensity data. The photoelectron pulses from the five PMT's are amplified (Gain = 5) and sent to photon counters, which output NIM level pulses. Constant fraction discriminators convert the NIM pulses to 10 ns wide TTL level pulses that are counted by a counter-timer board. Typical photoelectron count rates for this work were on the order of 1 MHz. A PC-based data acquisition system was used to record the signals from the PMT's. Each signal channel was digitized at a 10 kHz sampling rate for 10 seconds, resulting in 100,000 samples per channel. The intensity information from the Fabry-Perot fringe sampling is used to obtain temperature measurements. The density measurement is much simpler since it requires only an overall intensity measurement and does not require the FPI for spectral analysis. Therefore, a beamsplitter located just in front of the FPI input directs

approximately 10% of the incoming Rayleigh scattered light to a lens (L12), which focuses the light into a single PMT for density measurement. This PMT is labeled 5 in figure 6b.

A PID feedback control unit is used to adjust and maintain the jet total temperature to within +/- 1.5 K of the setpoint temperature. During stabilization of the FPI, while the laser beam is blocked from the probe volume, a linear actuator places a fine-wire (0.25 mm diameter) open-bead type K thermocouple into the flow to provide jet static temperature data. A pressure gauge measures the ambient (static) pressure approximately 10 mm away from the thermocouple location. Density information is derived using ideal gas law. The centerline axial velocity was evaluated using the total pressure measured with a pitot probe so that the jet velocity profile is known and the expected velocity fluctuations can be estimated.
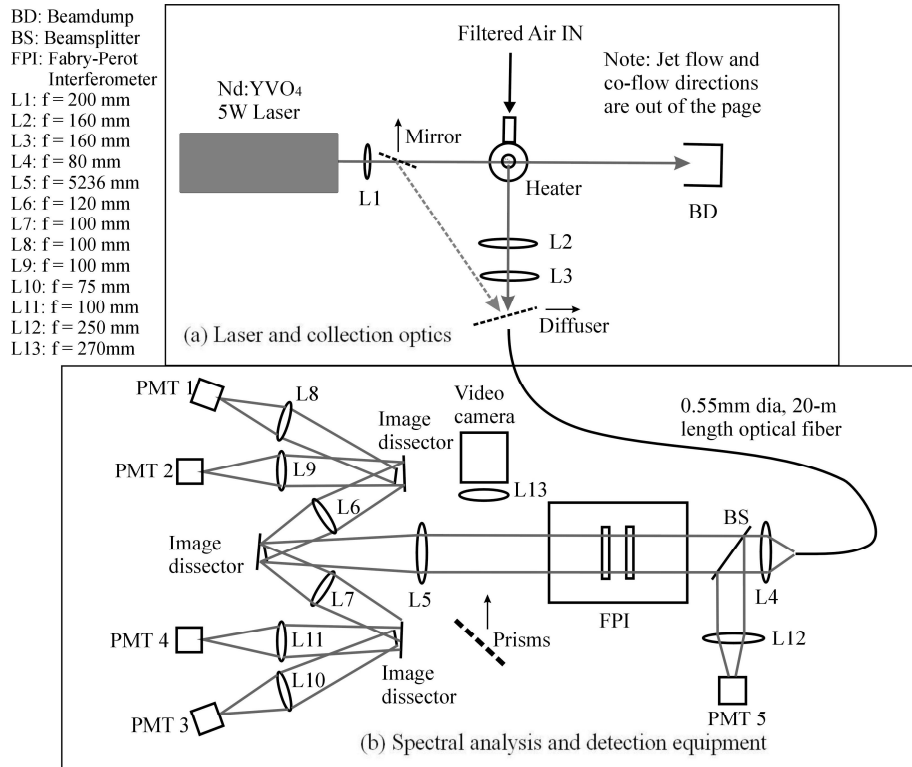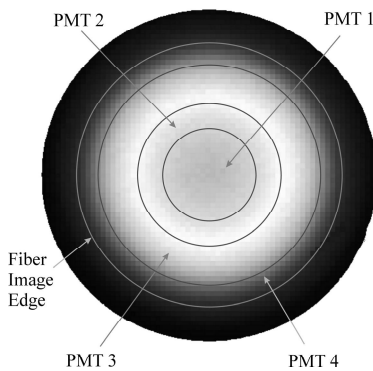
BD: Beamdump
BS: Beamsplitter
FPI: Fabry-Perot
     Interferometer
L1: f = 200 mm
L2: f = 160 mm
L3: f = 160 mm
L4: f = 80 mm
L5: f = 5236 mm
L6: f = 120 mm
L7: f = 100 mm
L8: f = 100 mm
L9: f = 100 mm
L10: f = 75 mm
L11: f = 100 mm
L12: f = 250 mm
L13: f = 270mm

Filtered Air IN

Note: Jet flow and co-flow directions are out of the page

Nd:YVO₄
5W Laser

Mirror

Heater

BD

L1

L2

L3

Diffuser

(a) Laser and collection optics

PMT 1

L8

Video camera

Image dissector

0.55mm dia, 20-m length optical fiber

PMT 2

L9

L6

Image dissector

L13

BS

L5

FPI

L4

L7

Prisms

L12

PMT 4

L11

Image dissector

L10

PMT 5

PMT 3

(b) Spectral analysis and detection equipment

Figure 6. Experiment schematic.

PMT 2

PMT 1

Fiber Image Edge

PMT 3

PMT 4

Figure 7. Dissection of a Fabry-Perot fringe pattern into four annular regions.

Fringe Amplitude
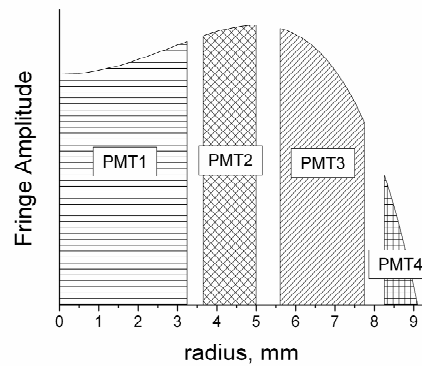
PMT1

PMT2

PMT3

PMT4

radius, mm

Figure 8. Radial slice of a Fabry-Perot fringe pattern showing the areas sampled by the four PMTs. Gaps between each area indicate regions of light loss during the dissection process.

4. RESULTS

4.1. Calibration

The technique was calibrated by operating the jet at temperatures ranging from 298 K to 550 K. The gas temperature and density were determined from thermocouple and pressure probe measurements. Since thermocouples measure the temperature of the metal probe bead rather than the gas temperature, there may be a difference between the actual gas temperature and the thermocouple measurement. These differences result from conduction losses down the thermocouple wire and radiation losses to the surroundings. The error in gas temperature was estimated to be less than ± 3 K for the relatively low temperatures studied here. The mean photon counts for the five PMT's were determined as a function of air density and temperature. The photon counts are linearly related to density as shown by the calibration curve in Figure 9. The amount of light in each of the four annular regions detected by PMT's 1-4 is a function of both density and temperature. By using a ratio technique, the dependence on density is removed. The ratios selected were PMT 3/PMT 4, to monitor changes in fringe width on the outer edge of the fringe pattern, and PMT 2/PMT 1, to monitor fringe width from the inner edge. Velocity changes cause a shift in the radial location of the fringe. The radial velocity component in this experiment is approximately zero, resulting in a nearly constant fringe diameter. Changes in fringe diameter due to velocity fluctuations, drift in the interferometer mirror spacing, or laser frequency drift, may cause some measurement error. Re-stabilizing the interferometer mirrors between every measurement minimizes the error due to mirror and laser frequency drift. Based on the mean axial velocity of 4.8 m/s, the magnitude of the radial velocity fluctuations is on the order of 0.5 m/s. Velocity fluctuations of this magnitude should have minimal effect on the temperature measurements. Figure 10 shows temperature as a function of the photon count ratio of PMT 3 to PMT 4. The ratio of PMT 2 to PMT 1 had very little change over this temperature range; therefore, it was neglected in this analysis. A second order exponential decay function was fit to the temperature versus PMT 3/PMT 4 curve. Due to the asymptotic nature of such a fit, the technique was extremely sensitive to intensity ratio changes at high temperatures but very insensitive at lower temperatures. The equations shown in figures 9 and 10 are used to calculate density and temperature at each data point to obtain time histories. The power spectra of the density and temperature fluctuations can be calculated from this information. Because of the high noise levels, it is necessary to use relatively long data records and calculate power spectra using a technique such as the Welch method of modified periodograms, which will be discussed in Sec. 4.3.
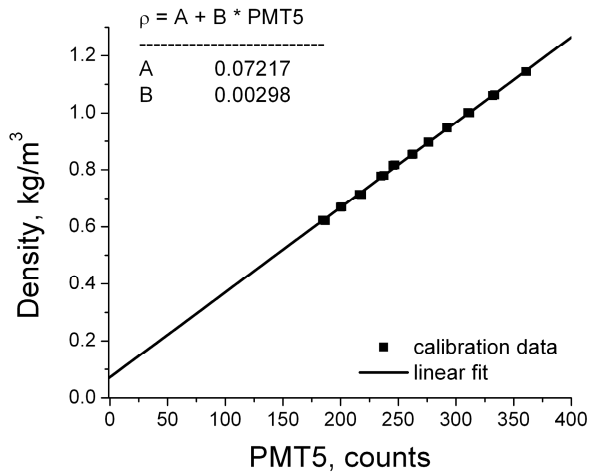

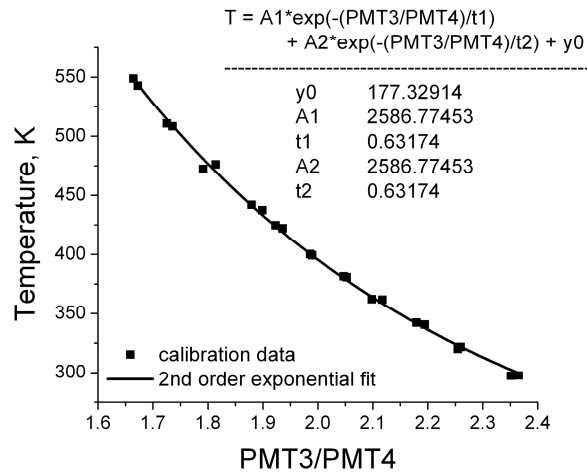Figure 9. Density as a function of photoelectron counts detected by PMT 5.

Figure 10. Temperature as a function of photoelectron count ratio of PMT 3 to PMT 4.

4.2. Jet temperature profiles

The Rayleigh probe volume is scanned radially at a single axial station through the center of the jet flow at two different temperatures to demonstrate the technique and provide temperature profiles. This scan provides temperature and density measurements in the jet core as well as in the turbulent mixing layer formed between hot and cold air streams. Figures 11 and 12 show temperature profiles for flows with centerline temperatures of 378 K and 483 K, respectively. The non-dimensionalized probe position is given in terms of radial location divided by jet exit diameter, *r/D*. Temperatures obtained from the Rayleigh technique using PMT 3/PMT 4 photon count ratios are shown as circle symbols while thermocouple measurements are shown by triangle symbols for comparison. Simultaneous density measurements were also obtained in these scans from PMT 5 photon count data. The temperatures shown as square symbols in figures 11 and 12 were calculated from these density measurements using the ideal gas law. All three independent temperature measurements compare quite well. Figure 11 contains information from two scans performed on different days using a single calibration, indicating good repeatability characteristics. Figure 13 shows the differences between the temperatures obtained from the Rayleigh technique and the thermocouple. The standard deviation shows that the error in *mean* temperatures is approximately +/- 7 K, while the standard deviation of the *individual* temperature measurements is similar to the Cramer-Rao lower bound estimate calculated in Sec. 2.2.
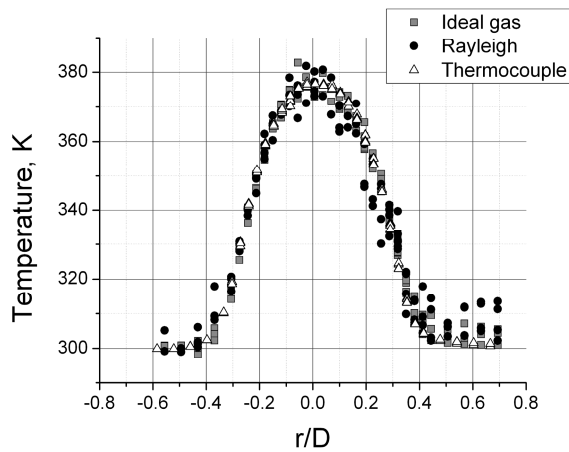

Figure 11. Temperature versus *r/D* in a heated round jet with centerline velocity and temperature of 4.7 m/s and 378 K.
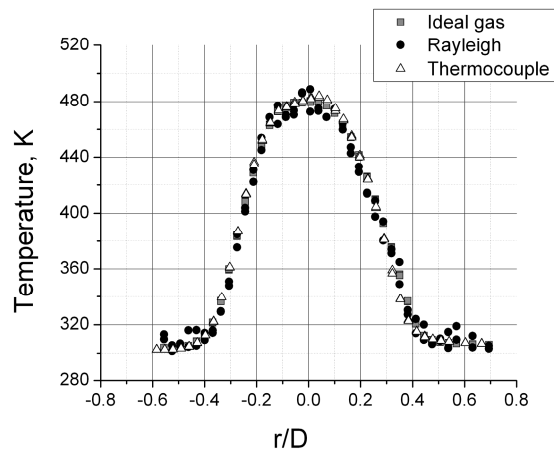

Figure 12. Temperature versus *r/D* in a heated round jet with centerline velocity and temperature of 5.3 m/s and 483 K.
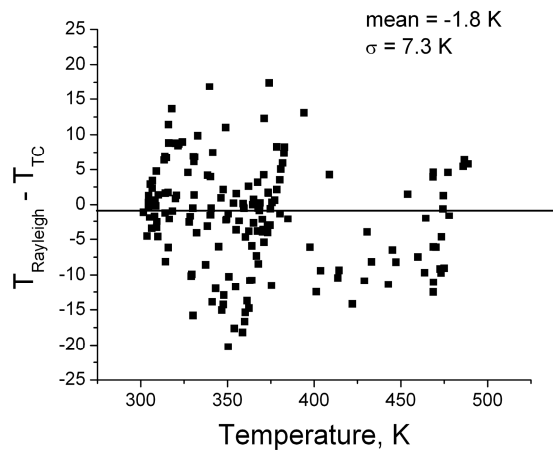

Figure 13. Error in Rayleigh temperature measurements compared with thermocouple measurements at the same location for the radial scans of figures 11 and 12 as a function of temperature.

4.3. Power Spectral Density (PSD) calculations

We used the Welch method of modified periodograms[17] to calculate an estimate of the power spectral density (PSD) of the density and temperature fluctuations. In this procedure, a long data record sampled at a rate f_s = 10 kHz for time t = 10 sec (total samples = $N = tf_s$) is subdivided into a number K_r = 389 of smaller records of length L = 512 samples, which are overlapped by 50%. The modified periodograms of each sub-record are calculated using a data window. These individual periodograms are then averaged to obtain the estimate of the power spectrum. The frequency resolution of the resulting spectrum is f_s/L = 19.53 Hz. Overlapping the segments by 50% provides a near maximum reduction in the variance in the spectral estimate. The resulting power spectrum provides fluctuation information out to 5 kHz. Figures 14 and 15 show normalized density and temperature PSD plots for a jet flow having a centerline velocity of 4.7 m/s and temperature of 378 K. The shot noise contribution has been subtracted from each spectrum since the shot noise contributes approximately equally over all frequencies. In each figure, spectra are shown for three radial measurement locations: centerline (r/D = 0), shear layer (r/D = 0.3), and a region outside the mixing layer (r/D = 0.7). As expected, the highest fluctuations are found in the shear layer, where the higher temperature air from the jet core is mixing with the colder co-flow air. The spectra at the other two locations are relatively flat. Figures 16 and 17 show similar PSD plots for a jet having a centerline velocity and temperature of 5.3 m/s and 483 K.

The cross-spectra between density and temperature records were also calculated. When the cross-spectra are calculated, any noise, such as shot noise that is uncorrelated will be removed from the spectrum. The coherence is the real part of the cross-spectrum and is a measure of how well the two measurement records correlate at a given frequency. The phase is the imaginary part of the cross-spectrum. Cross-spectra between density and temperature fluctuations for jet centerline temperatures of 378 K and 483 K are shown for a shear layer radial location in Figures 18 and 19. A coherence of 1.0 indicates perfect correlation between the fluctuations of density and temperature. The measurements show coherence of about 0.5 and 0.7 in the frequency range of 0-500 Hz for the low temperature and high temperature flows, respectively. There is no phase lag (phase = 0) since both temperature and density are measured simultaneously at the same location. By recording sound pressure fluctuations using microphones and following a similar cross-spectral analysis, correlations between sound pressure fluctuations and either density or temperature fluctuations can be obtained. Information of this type is useful to aero-acoustic researchers studying the sources of noise generation in jets.
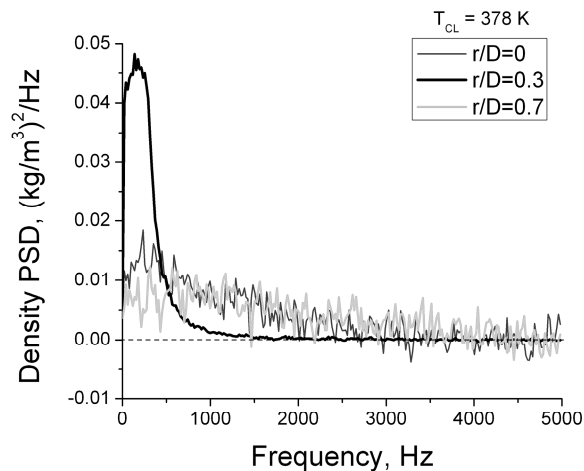

Figure 14. Normalized power spectrum of density fluctuations at three radial locations in jet with centerline velocity and temperature of 4.7 m/s and 378 K.
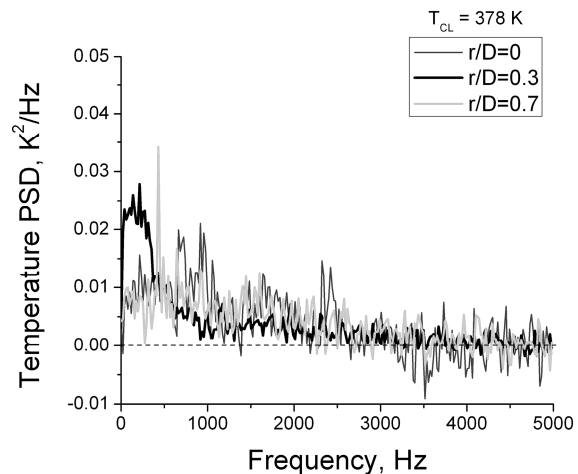
Figure 15. Normalized power spectrum for temperature fluctuations at three radial locations in jet with centerline velocity and temperature of 4.7 m/s and 378 K.
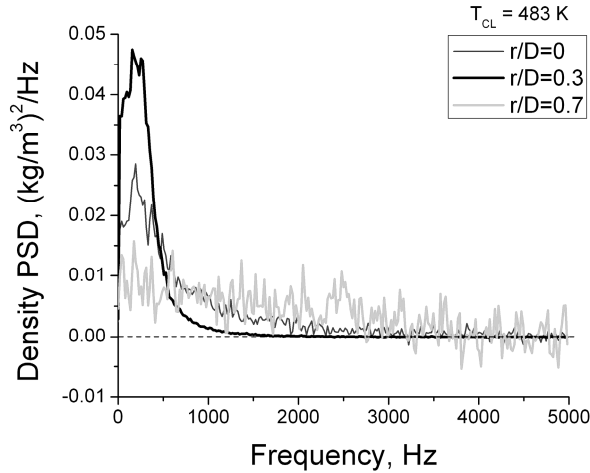
Figure 16. Normalized power spectrum of density fluctuations at three radial locations in jet with centerline velocity and temperature of 5.3 m/s and 483 K.
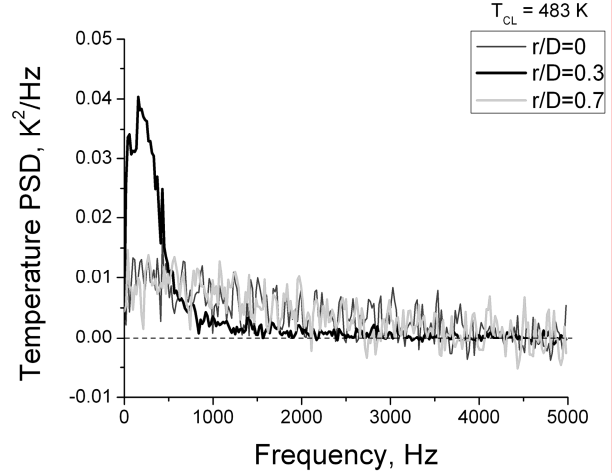

Figure 17. Normalized power spectrum for temperature fluctuations at three radial locations in jet with centerline velocity and temperature of 5.3 m/s and 483 K.
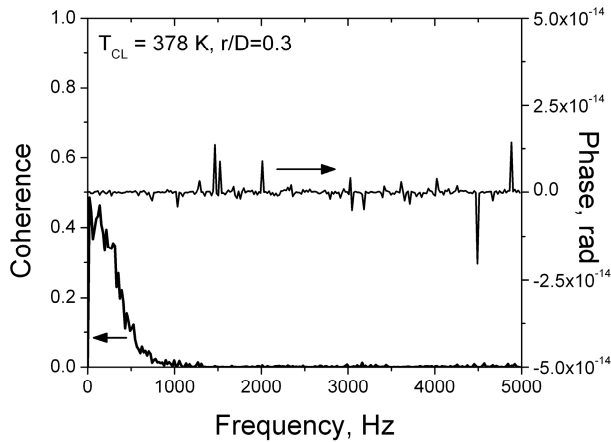

Figure 18. Normalized cross-spectra between density and temperature fluctuations at r/D=0.3 in jet with centerline velocity and temperature of 4.7 m/s and 378 K.
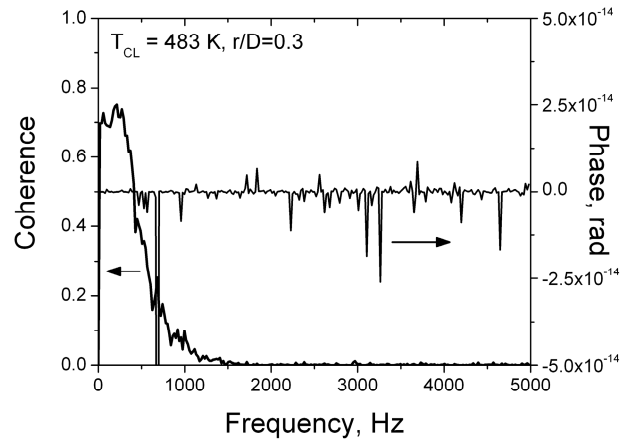

Figure 19. Normalized cross-spectra between density and temperature fluctuations at r/D=0.3 in jet with centerline velocity and temperature of 5.3 m/s and 483 K.

5. CONCLUDING REMARKS AND FUTURE WORK

A technique for obtaining dynamic gas density and temperature measurements using molecular Rayleigh scattering was described. Density was determined from an overall intensity measurement of the scattered light, while temperature was determined by analyzing the scattered light with a Fabry-Perot interferometer. The signals from five photomultiplier tubes were simultaneously recorded using photon counting electronics operating at 10 kHz sampling rate with 10 second recording periods. An uncertainty analysis was presented that demonstrated a lower bound of about 31% for individual temperature measurements and about 3.8% for individual density measurements. The measurement uncertainty can be lowered significantly by increasing the number of detected photons. This may be done by using a higher power laser and/or by using higher quantum efficiency detectors. Density and temperature measurements taken in a low speed heated jet flow were presented. The measured standard deviation for mean temperature measurements was +/- 7 K. The standard deviation of the individual measurements was closer to the lower bound estimate. Temperature and density power spectra were obtained using the Welch method of modified periodograms. The presented Rayleigh scattering technique simultaneously measures time history of density and temperature flow fluctuations and should provide a valuable research tool for the study of noise generation in turbulent flows.

Several methods for improvement of this technique were realized from this experiment. In future work, the radius of the reference fringe and/or the fringe dissection arrangement may be changed so that the two inner annular segments are more sensitive to temperature changes. This will provide an additional independent measure of temperature that can be averaged together with temperatures obtained by the current method (ratio of outer two regions) to lower measurement uncertainty. Also, the cross-spectrum of the two temperature measurements can be used to remove the shot noise contribution from the power spectrum. A significant amount of light is currently lost in the transmission between image dissectors due to the thickness of the smaller mirror and the angles between the two mirrors. Using an annular detector or a more efficient method of dissecting the fringe image should decrease measurement uncertainty and improve the technique's signal to noise ratio. High quantum efficiency annular or rectangular array detectors will be explored. Eventually this technique will be extended to measure velocity fluctuations simultaneously with temperature and density fluctuations. In this case, a ratio method will probably not be sufficient for analysis since the ratio is a function of both temperature and velocity. A least-squares technique will be necessary to extract the desired information from the photon count data in the concentric regions.

ACKNOWLEDGEMENTS

REFERENCES

1. Eckbreth, A.C., *Laser Diagnostics for Combustion Temperature and Species*, pp. 162-361, Ababus Press, Cambridge, 1988.
2. Cummings, E.B., *Laser-Induced Thermal Acoustics*, PhD Dissertation, California Institute of Technology, Pasadena, 1995.
3. Hart, R.C., Balla, R.J., Herring, G.C., "Nonresonant referenced laser-induced acoustics thermometry in air," Appl Optics, **38**, 577-584, 1999.
4. Li, Y., Roberts, W.L., Brown, M.S., "Investigation of gaseous acoustic damping rates by Transient Grating Spectroscopy," AIAA Journal, **40**, 1071-1077, 2002.
5. Seasholtz, R.G., and Greer, L.C., "Rayleigh Scattering Diagnostic for Measurement of Temperature and Velocity in Harsh Environments," AIAA paper 98-0206, 1998.
6. Panda, J., and Seasholtz, R.G., "Velocity and temperature measurement in supersonic free jets using spectrally resolved Rayleigh scattering," AIAA paper 99-0296, 1999.
7. Mielke, A.F., Seasholtz, R.G., Elam, K.A., and Panda, J., "Time-average measurement of velocity, density, temperature, and turbulence velocity fluctuations using Rayleigh and Mie scattering," accepted for publication in Exp in Fluids, published online first, 24 May 2005.
8. Lock, J.A., Seasholtz, R.G., John, W.T., "Rayleigh-Brillouin scattering to determine one-dimensional temperature and number density profiles of a gas flow field," Appl Optics **31**, 2839-2848, 1992.
9. Seasholtz, R.G., and Panda, J., "Rayleigh scattering diagnostic for dynamic measurement of velocity and temperature," AIAA paper 99-0641, 1999.
10. Seasholtz, R.G., Panda, J., and Elam, K.A., "Rayleigh scattering diagnostic for measurement of velocity and density fluctuation spectra," AIAA paper 2002-0827, 2002.
11. Tenti, G., Boley, C.D., Desai, R.C., "On the kinetic model description of Rayleigh-Brillouin scattering from molecular gases," Can J Phys, **52**, 285-290, 1974.
12. Sandoval, R.P., Armstrong, R.L., "Rayleigh-Brillouin spectra in molecular nitrogen," Phys Rev A, **13**, 752-757, 1976.
13. Yip, S., Nelkin, M., "Application of a kinetic model to time-dependent density correlations in fluids," Phys Rev, **135**, A1241-A1247, 1964.
14. Boley, C.D., Desai, R.C., Tenti, G. "Kinetic models and Brillouin scattering in a molecular gas," Can J Phys, **50**, 2158-2173, 1972.
15. Vaughan, J.M., *The Fabry Perot Interferometer, History, Theory, Practice, and Applications*, pp. 89-134, Adam Hilger, Bristol, 1989.
16. Whalen, A.D., *Detection of Signals in Noise*, pp. 325-331, Academic Press, New York, 1971.
17. Welch, P.D., "The use of fast Fourier transform for the estimation of power spectra: A method based on time averaging over short, modified periodograms," IEEE Trans on Audio and Electroacoustics, **AU-15**, 70-73, 1967.